Innovative Feuchtemessung in Forschung und Praxis

Berichtsband zur 10. CMM-Tagung
Innovative Feuchtemessung in Forschung und Praxis –
Materialeigenschaften und Prozesse
Karlsruhe, 10.– 11. Oktober 2019

Herausgegeben von
Rainer Schumann
CMM, Karlsruher Institut für Technologie

Unter Mitarbeit von
Anke Ehbrecht
Katja Emmerich
Franz Königer
Stephan May

Inhaltsverzeichnis

Themenschwerpunkt: Messtechnik in ausgewählten Anwendungen

HF-Technik & Sensorik

Themenschwerpunkt: Wasser und mineralische Materialien

Angewandte Mineralogie

Themenschwerpunkt: „P-Recycling - Quo vadis”?

Umwelt-technologie

Themenschwerpunkt: „Qualität der P-Recyclate”

Umwelt-technologie

Themenschwerpunkt: Rückgewinnungsverfahren

Umwelt-technologie

HF-Technik & Sensorik

Dielectric Sensor & Methods

Themenschwerpunkt:
Messtechnik in ausgewählten
Anwendungen

Correlation between the electric impedance and the water layer thickness in partially saturated screed samples

C. Strangfeld[1], H. Stolpe[1], S. Kruschwitz[1,2]

[1] Bundesanstalt für Materialforschung und -prüfung, Unter den Eichen 87, 12205 Berlin, Germany

[2] Technische Universität Berlin, Gustav-Meyer-Allee 25, 13355 Berlin, Germany

Keywords: material moisture, screed, embedded sensors, electric impedance, water layer thickness

Abstract

The moisture content of screed samples is monitored by means of embedded sensors. Relative humidity sensors and multi-ring-electrodes are used to measure the spatial moisture distribution during desorption. Based on the humidity data and the pore volume distribution, the moisture and the water layer thickness within the pore space are predicted. Slit shape as well as cylindrical pores are evaluated. Finally, the measured real part of the electrical impedance and the calculated water layer thickness are correlated. Based on the available data, a significant trend change of the impedance is documented at a water layer thickness of approximately 3 nm. This water layer thickness corresponds to a relative humidity of 88.3%.

Zusammenfassung

Die Materialfeuchte von Estrichproben wird mittels eingebetteter Sensorik verfolgt. Relative Luftfeuchtesensoren als auch Multi-Ring-Elektroden werden verwendet, um tiefenaufgelöst die Feuchteverteilung während der Desorption zu messen. Basierend auf den Daten der relativen Luftfeuchte und der Porenvolumenverteilung werden die Materialfeuchte und die Wasserfilmdicke vorhergesagt. Schlitzporen als auch Zylinderporen werden als Porenmodelle für die Auswertung zu Grunde gelegt. Der gemessene Realanteil der elektrischen Impedanz und die vorhergesagten Wasserfilmdicken werden korreliert. Basierend auf den vorhandenen Daten zeigt sich eine deutliche Trendveränderung der Impedanz bei einer Wasserfilmdicke von ca. 3 nm. Diese Wasserfilmdicke stellt sich in dem untersuchten Porensystem bei einer relativen Luftfeuchte von 88.3% ein.

Contact address:
Christoph Strangfeld
Bundesanstalt für Materialforschung und -prüfung,
Unter den Eichen 87,
12205 Berlin, Germany
Phone: +49 (0) 81 04 - 42 73
Email: christoph.strangfeld@bam.de
Homepage: www.bam.de

1 Motivation

Moisture and moisture transport in concrete are important factors controlling the durability of cementitious building materials. In order to identify deterioration mechanisms non-destructively, different ways of measuring the electrical resistivity have been studied for many years. In most cases these works focused on the direct current (DC) electrical properties to do one of the following: determine absolute moisture contents, monitor moisture transport, or capture information on ongoing (electro-)chemical reactions like chloride ingress, alkali-silica-reaction (Weise et al., 2012), or corrosion (Nürnberger, 1995) (Kruschwitz, 2007). In the 1990s, so-called multi-ring electrode (MRE) had been developed by the IBAC institute in Aachen (Sodeikat, 2010) in order to identify moisture distributions on the surface near mainly water exposed structures. This probe uses an optional number of stacked layers of electrodes and allows the monitoring of moisture distributions according to transport phenomena. In the dry state, building materials acts like insulators and the measured resistivity may vary over several orders of magnitude depending on the saturation degree, type of fluid in the pore system, temperature etc. and, as the electrical resistivity is very sensitive, to moisture variations. Thus, it is often assumed to be a useful indirect indicator for condition assessments and service life prediction (Morris et al., 2002).

A completely different type of sensor for measuring moisture contents in porous building materials are relative humidity probes. These are based on hygric measurements of the amount of gaseous moisture in a pore system. Depending on the specific material and the shape of the pores, the amount of relative humidity and the liquid water content within a system are interrelated.

Measuring the electrical resistivity as well as the relative humidity can be very sensitive methods, but the results for both are affected by a number of unknown boundary conditions. The joint interpretation of sensors based on different physical principles and, therefore, yielding complementary information, can significantly reduce the ambiguity of the measured results. Following this mindset in this paper we present the combined use of a multiring electrode and, in the same way, stacked relative humidity sensors to monitor the drying behaviour of floor screeds. Until now,

there were only destructive testing methods to determine the critical (low) water content for laying floors. The goal of this study is to first learn about the sensitivities of the probes used to evaluate the signals depending on the moisture content and the calculated water film thickness along the pore surfaces.

2 Experimental setup and water layer thickness calculation

To begin, the screed samples and their storage in the climate chamber are discussed. Then, the embedded humidity sensors as well as the multi-ring-electrodes are considered in detail. Eventually, the pore size distributions are determined by mercury intrusion porosimetry and gas adsorption.

2.1 Screed samples

In the current study, four cement-based (CT) and four calcium-sulphate-based (CA) screed types are investigated during the hydration and evaporation process. The different screed types and their characteristic values of material properties are listed in (Strangfeld and Kruschwitz, 2018). For each screed type, two samples, one of 35 mm and one of 70 mm thickness, are equipped with embedded sensors. All samples are cylindrical with an inner diameter of 300 mm and are sealed at the bottom and sides in order to ensure a symmetric moisture transport. The casings are polyvinyl chloride (PVC) sewage pipes with a wall thickness of 7.7 mm. A transparent polyethylene foil is used as bottom material. The foil itself is stapled directly on the PVC pipe and sealed with a polymer based sealant. The materials are chosen to minimise moisture diffusion through the casing or the foil. A floating screed floor construction is simulated by placing the samples on top of styrodur (20 mm), styrofoam (40 mm), and washed out concrete (40 mm).

All screed samples are manufactured during a one-day period. For each screed type, the water/cement ratio recommended by the producer is used. All weights are checked by a high precision balance before mixing. After concreting, the samples are covered and stored overnight in the

production room (at approximately 295 K). On the following morning, the samples are stored in a ventilated climate chamber at an ambient relative humidity of h = 50% rH and an ambient temperature of T = 296 K. The storage of the samples in the climate chamber and the evolution of the ambient conditions in the climate chamber are shown in (Strangfeld et al., 2016). In the following, the unit of the relative humidity is rH.

2.2 Embedded humidity sensors

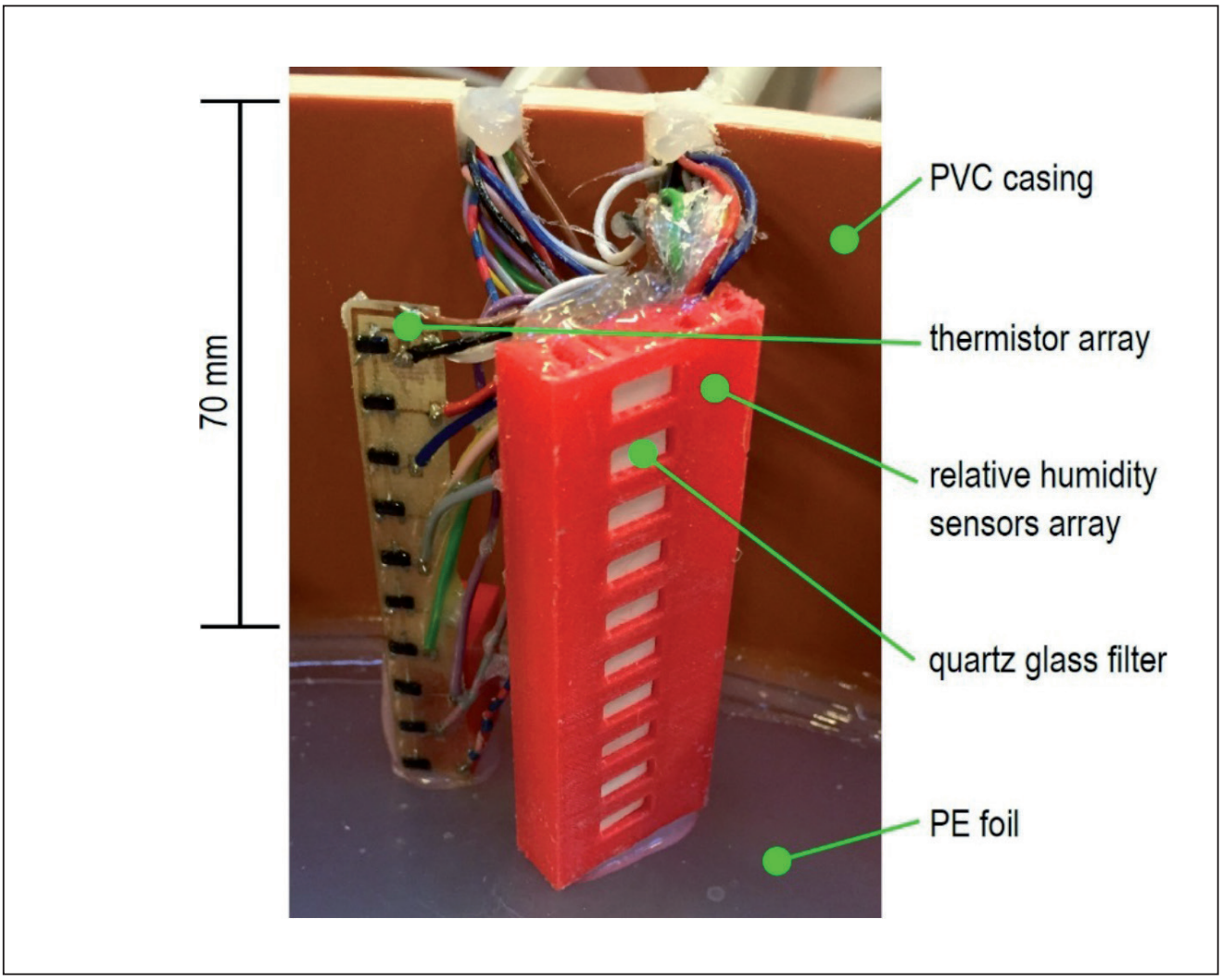

Fig. 1: Embedded thermistor array and embedded relative humidity sensor array before concreting; both arrays have ten measurement position with a spatial resolution of 6 mm

Fig. 1 presents the setup of the embedded sensors. The wired temperature and relative humidity arrays consist of ten individual sensors in the thick samples and five sensors in the thin samples (Hase, 2016). The temperature sensors are MCP9700A three-pin thermistors in surface mounted device (SMD) design. They are installed directly on the board and all are covered by epoxy resin. The relative humidity sensors

HIH-5031 are in SMD design as well. Within the range of 11% rH ≤ *h* ≤ 89% rH, the humidity sensor HIH-5031 has a declared accuracy of ±3% rH, including interchangeability. Below 11% rH and above 89% rH, the accuracy amounts to 7% rH including a reversible hysteresis of 3% rH. The overall repeatability for one single sensor is declared with 0.5% rH based on the data sheet. The sensors are mounted on the board and then placed in the orange casing. Thereby, the casing fulfils two tasks. On the one hand, each sensor gets its own separated housing inside the casing. This inhibits any air or moisture convection through the array. On the other hand, the casing positions the sensors directly behind the quartz glass filter. These filters are necessary in order to prevent direct contact of the humidity sensor membrane from water and screed mixture during concreting. The open area of the filter is 3.3 mm times 7.3 mm. Thus, the measured humidity is the average over this area. The centre of the filter is considered as the representative measurement position. The backside of the casing is also covered with epoxy resin. The humidity sensors are placed at vertical distances of 6 mm and the lowest humidity sensor is 8 mm above the bottom. After concreting, the sensor arrays and the cables are completely surrounded and overlaid by screed. Thus, the top surface of the screed is a homogeneous, clean, and closed surface to minimise the influence of the embedded sensors. Two USB-6210 data acquisition systems from “National Instruments“ with a 16-bit resolution are used to record the data from the embedded sensors. All discussed humidity values in this study are temperature compensated. The corresponding measurement data are available online (Strangfeld et al., 2018).

A high precision balance with a maximum load of 72 kg and an accuracy of 0.1 g is used as reference measurement system. All screed samples are weighed at each measurement day.

These gravimetric measurements provide a precise and reliable reference of the average water content of each sample and holds as reference for the predicted total free liquid water in the pores. The corresponding measurement data are available online (Strangfeld et al., 2018).

2.3 Embedded multi-ring-electrodes

Fig. 2: Embedded multi-ring-electrode before concreting

Fig. 2 shows a multi-ring-electrode for thin samples. The entire electrode has a diameter of 19 mm and a height of 32 mm. It consists of eight stainless steel spacers with a height of 2 mm. Between two adjoining electrodes spacers are placed. The spacers are made of polylactide with a high of 1.7 mm. This geometry results in a spatial resolution of 3.7 mm, including seven measurement positions. The middle of the polylactide spacer between two adjoining electrodes is assumed as the corresponding measurement position. Nevertheless, the measurement volume includes the two electrodes, the spacer, and the screed in the vicinity of the electrodes. After concreting, the topmost position is located at 7.4 mm depth and the lowest measurement position is approximately 29.6 mm depth. Inside the electrode, all eight electrodes are electrically connected. At the end of the manufacturing process, the inner volume of the multi-ring-electrode is filled with epoxy resin. This covers the solder point from the screed and protects them against corrosion and mechanical damages. Detailed construction drawings are given in (Hase, 2016). After concreting, the multi-ring-electrode and its cable are completely embedded in the screed. Thus, the top surface of the screed is homogeneous, clean, and closed to minimise the influence of the embedded sensors. The data are acquired by the inductance, capacitance, resistance (LCR) meter HM 8118 of the company Hameg.

2.4 Pore volume distribution

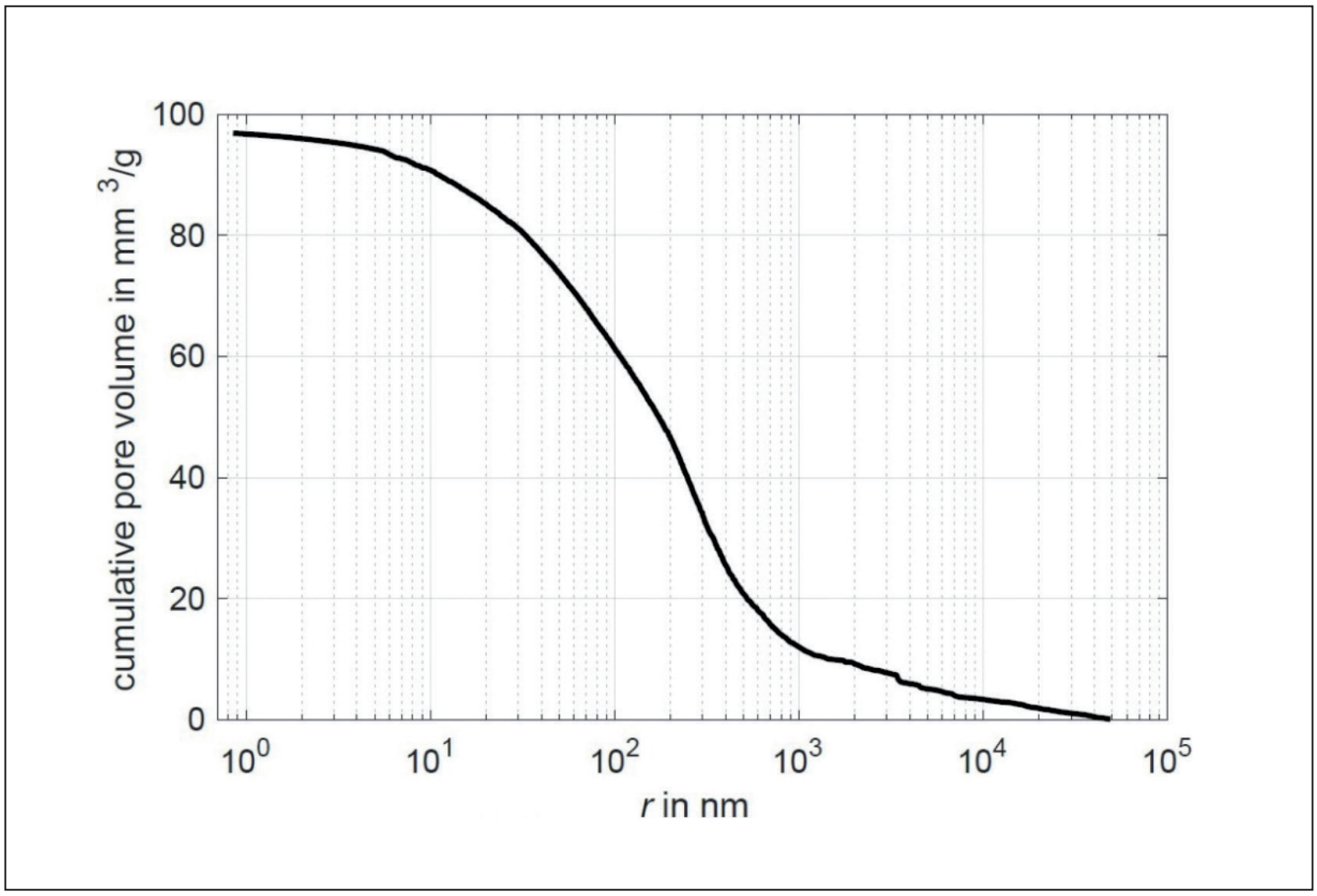

Fig. 3: Cumulative pore size distribution of the investigated cement based floating screed, data are based on gas adsorption and mercury intrusion porosimetry

Fig. 3 illustrates the cumulative pore volume for the cement based floating screed. These pore distributions are based on a combination of mercury intrusion porosimetry and gas adsorption (ISO, 2006) (DIN, 1998). The mercury intrusion porosimetry generates test pressures between 0.01 MPa and 400 MPa. The conversion from pressure to a certain pore radius includes the Washburn equation (Washburn, 1921). The measurement procedure is the exact reproduction of the international standard (ISO, 2006). The calculated pore radius starts at approximately 50 µm and sensitivity is recorded to a minimum pore radius of approximately 2 nm. The used dry sample masses are between 0.8 g and 1.5 g and the model assumes cylindrical pores to convert pressure into pore sizes. The other used method is gas adsorption (DIN, 1998) based on the physisorption of nitrogen gas at 77 K in a pressure range of 4.5 mbar to 1 bar. The conversion from pressure to a certain pore diameter is based on the Barrett-Joyner-Halenda theory (Barrett et al., 1951). This theory includes

the layer thickness of the adsorbed nitrogen according to Halsey (Halsey, 1948) and the Kelvin equation for calculating the pore radius. The sample mass varies between 1 g and 4.5 g. The measurement procedure is the exact reproduction of the international standard (ISO, 2006). The measured pore radii are between 0.9 nm and 100 nm. At small pore radii, 0.9 nm to approximately 10 nm, the gas adsorption shows a significantly higher sensitivity as compared to the mercury intrusion. The corresponding measurement data are available online (Strangfeld et al., 2018).

The two porosimetry measurements are merged together to cover all pore radii. At pore radii of approximately 5 nm, most pressure steps of the mercury intrusion porosimetry cannot enter further pore volume. Thus, the pore volume of the associated pore radii becomes zero. This leads to a very wriggly pore size distribution. For these and smaller pore radii, the gas adsorption is considered to be more appropriate for our analysis. The point of too “wriggly“ mercury intrusion results depends on the material and is determined by eye. For the cement-based floating screed, gas adsorption results are used for radii between 0.85 nm ≤ r ≤ 5.55 nm. The gas adsorption results used in the chosen range consist of approximately 13 sampling points. Then, the mercury intrusion porosimetry with around 400 sampling points is added to a maximum pore radius of 85 µm. The investigated screed has a total porosity of around 20%. The pore distribution is uniform over the entire measured range and no dominant (modal) pore size can be determined. Furthermore, even the smallest measured pore radii still contribute significantly to the overall porosity.

2.5 Water layer thickness calculation of a partially saturated pore

In cement paste and screed, the moisture transport occurs in the pore system of the material. The mass balance adapted to moisture in porous materials describes the transport process. Thereby, a thermodynamic equilibrium between the free liquid water in the pores and the water vapour partial pressure is assumed. The thickness of the adsorbed water layer t_a in nm begins at the fringe of the pore. If the humidity increases, more water passes into the liquid state due to the increase of the water vapour pressure. The thickness of the adsorbed water layer increases and the pore fills up, which coincides with a higher pore saturation. Ba-

sed on the theory by Hillerborg, the resulting water layer is calculated by means of the two following equations (Chaube, 1994).

$$t_a = \frac{t_w h C_{md}}{(1 - \frac{h}{h_m})(1 - \frac{h}{h_m} + C_{md} h)} \quad (1)$$

$$h_m = exp(-\frac{\gamma M}{\rho_l R T (r - t_a)}) \quad (2)$$

C_{md} is a material constant related to the moisture diffusivity and adapted to cement based materials. t_w is the thickness of one monomolecular water layer in nm. R is the ideal gas constant in J/molK, t_a the temperature in K, M the molecular mass of water in kg/mol, and γ is the surface tension in N/m. During adsorption, the so called maximum humidity h_m is the humidity where the air volume in the centre of cylindrical pore disappears completely. The equations are based on the Kelvin equation and take into account the variation of the vapour pressure due to the curved liquid-vapour interface at the inner layer (Thomson, 1871). Hence, every pore radius possesses an individual maximum humidity h_m. For every pore radius, the saturation is known based on this approach. Hence, for cylindrical pores, the pore saturation is defined as follows:

$$s = 1 - (\frac{r - t_a}{r})^2 \quad (3)$$

Tab 1: Material parameters and properties used for free liquid water and water vapour at 296 K

Parameter	Numeric value	Unit
C	15	
M	0.018	kg/mol
R	8.314	J/mol K
t_w	0.35	nm
γ	0.722	N/m
ρ_l	997.54	kg/m^3

Tab. 1 recapitulates the used parameter to compute the pore saturation. All parameters are defined at a standard ambient pressure of p_0 = 101325 Pa and an ambient temperature of T = 296 K. A detailed description of computing the water layer thickness is given in (Strangfeld and Kruschwitz, 2018).

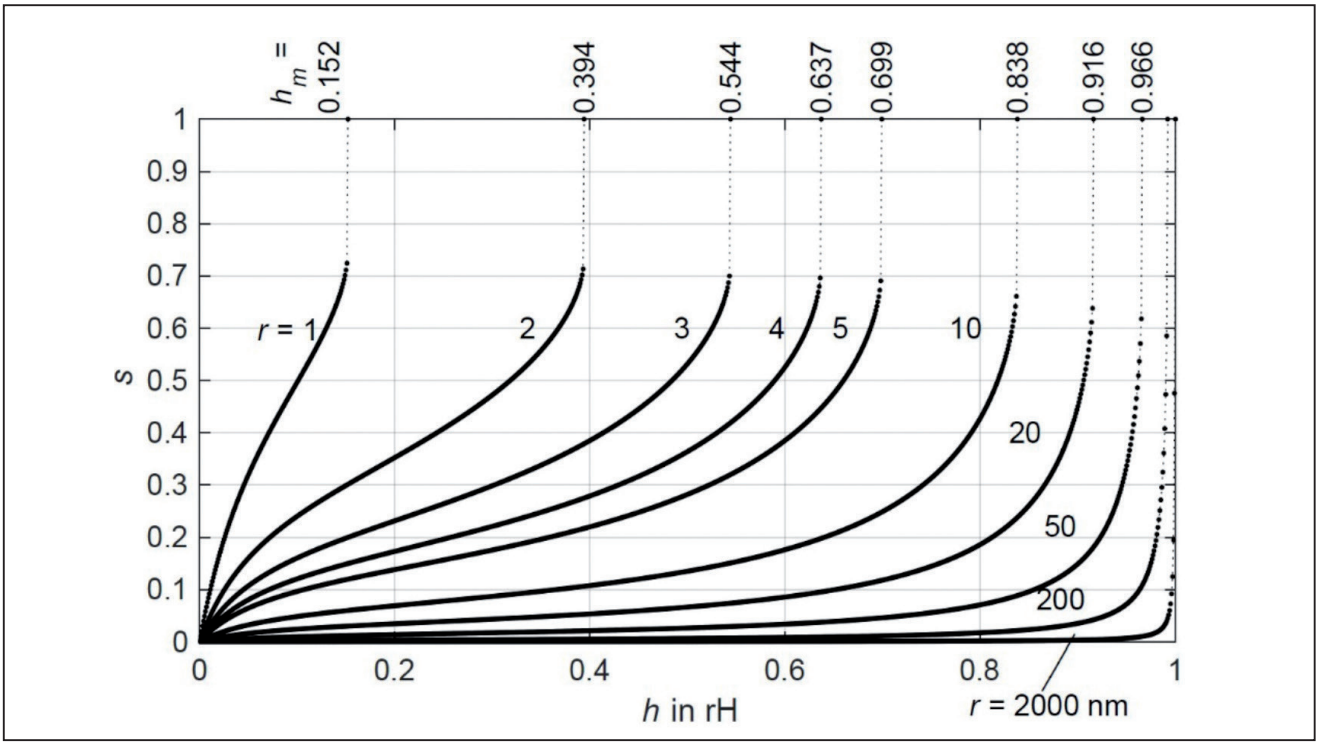

Fig. 4: Pore saturation of a single pore depending on the ambient relative humidity *h* based on the approach by Hillerborg; all pore radii are given in nm

Fig. 4 reveals the computed pore saturation based on the approach of Hillerborg (Hillerborg, 1985) for the parameters shown in **Tab. 1**. For cylindrical pores with pore radii between r = 1 nm and r = 2000 nm, the pore saturation s as a function of the humidity is illustrated. On top of the plot, the corresponding maximum humidity hm is depicted. For example, for a common ambient relative humidity of 50%, pores with r = 1 nm or r = 2 nm are already completely saturated. A pore with r = 10 nm is s = 13.5% water-filled and for r = 200 nm, the saturation is around s = 0.66%. For h > 0.95 rH, the increase of pore saturation is highly exponential, especially for larger pores. Thus, for high humidity, the measurement uncertainty becomes higher.

The capillary saturation S_{cp} is the summation of all pore saturation multiplied with the corresponding pore volume and the density of liquid water, resulting in the absolute water content (Strangfeld and Kruschwitz, 2018).

3 Data acquisition and evaluation

3.1 Processing of the humidity data

One embedded array for thin samples consists of five relative humidity sensors. The topmost sensor has a distance of around 6 mm to the top surface of the screed sample. The bottommost sensor has a depth of around 30 mm. The humidity is interpolated linearly to the measurement positions of the multi-ring-electrodes. This simple and ordinary approach of fitting the humidity data does not incorporate the high non-linear behaviour of convective and diffusive moisture transport. Nevertheless, this approach is used because of its high robustness. Non-linear interpolation, i.e. cubic splines, or extrapolation from the sensor position to the top surface or the bottom may give non-physical trends and values.

Furthermore, all measured humidity values have to be below 95% to be used for the absorbed water prediction. We assume that the measured pore volume distribution is representative for the entire sample and that the moisture transport is symmetric to the surface normal. The sample weight including embedded sensors is measured before concreting and always subtracted. Thus, the screed net weight is known. The cement based sample is oven drying at 378 K and an ambient relative humidity of less than 10% rH is maintained until a constant weight is reached.

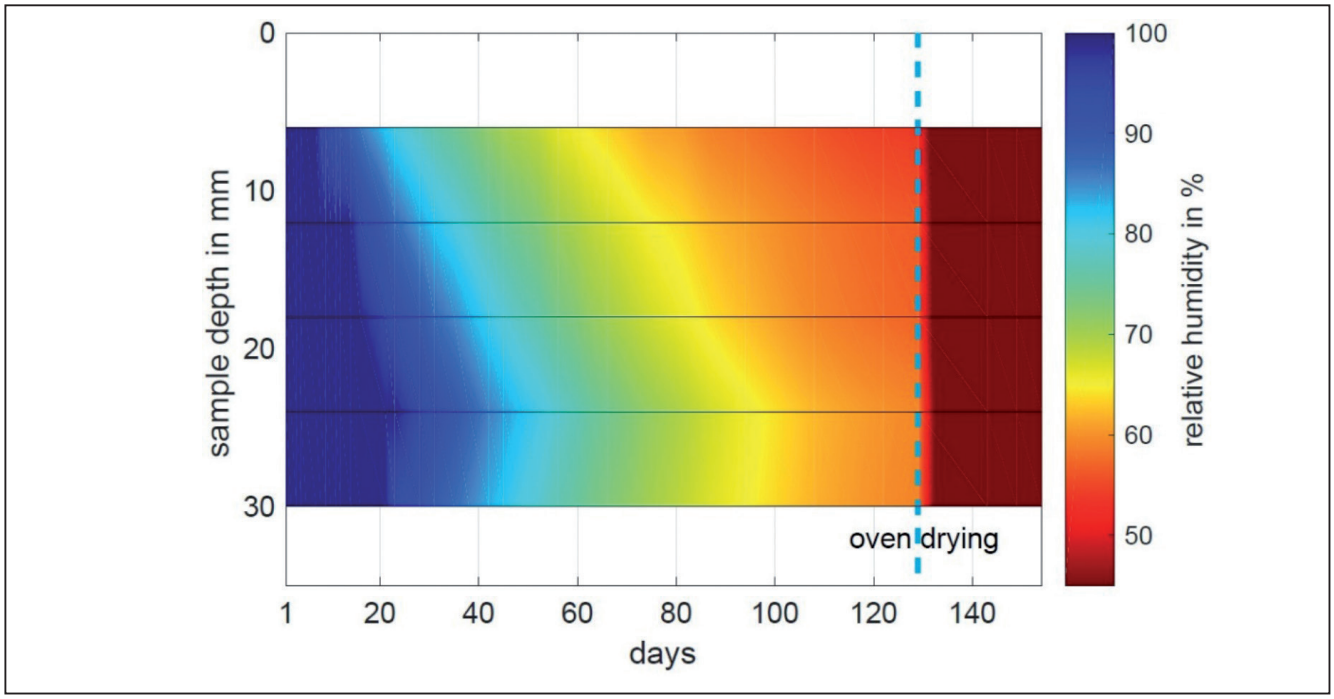

Fig. 5: Spatial and temporal distribution of the corresponding relative humidity for the cement based floating screed with 35 mm sample thickness presented as a two-dimensional contour plot

Fig. 5 shows the distribution of the relative humidity for a thin cement based floating screed sample over time. This contour plot represents the interpolated relative humidity based on 38 measurements. At the beginning, the embedded humidity sensors reach saturation in the fresh screed. On day 8, the topmost sensor leaves saturation. From then on, sensors start to leave saturation from top to bottom. A clear dehydration gradient is visible due to screed hydration and evaporation. On day 28, all sensors leave saturation. On day 129, the topmost sensor with h = 54% rH almost reaches the equilibrium moisture content of 50% rH predefined by the climate chamber humidity. The measurement on day 129 reveals a maximum of h = 59.4% rH in the sample. After this last measurement in the climate chamber, a period of 25 days of oven drying follows to determine the dry screed net weight and the corresponding moisture content in percent by weight.

3.2 Processing of the multi-ring-electrode data

For all measurements of resistors and capacitances of electrodes pairs, we use the LCR measuring bridge HM8118. **Fig. 6** shows the measurement instrument as a grey box, the equivalent circuit of connection cables and the device under test (MRE) represented as parallel resistor and capacitance of electrodes pairs.

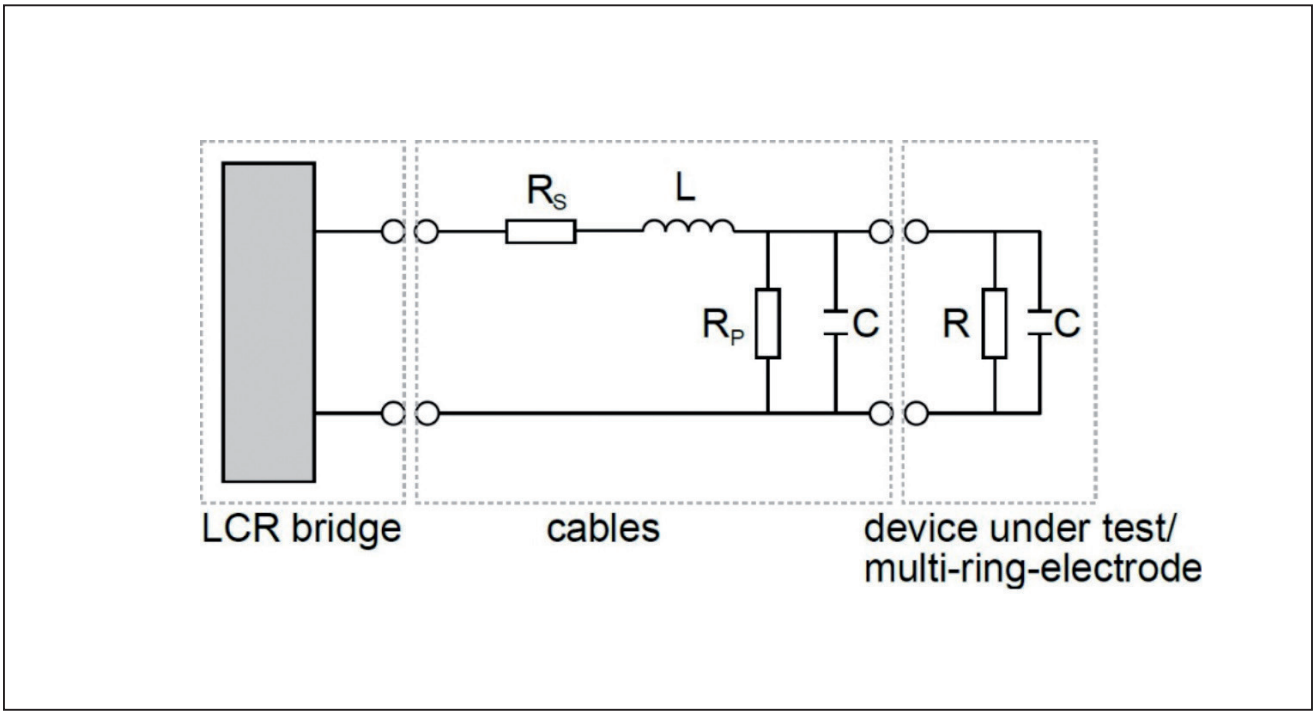

Fig. 6: Equivalent circuit diagram of the multi-ring-electrode measurements; including the device under test as well as the cables with their parallel resistance RP and serial resistance RS

To minimize measurement errors from cables and terminals residual inductances, capacitances, and resistances the LCR measuring bridge provide an open and short calibration procedure for all measurement frequencies. To detect the parallel resistance and capacitance of cable the measuring terminals must to be open, and to detect series resistance and inductance the terminals must be short. Furthermore, the LCR measuring bridge works with Kelvin measuring cables. The 4-wire method is necessary to measure smallest capacitances and resistors.

Because we have 7 electrode pairs for one multi-ring-electrode, we use a switching matrix. In the current study, the connection cables between switching matrix and the MRE simply consists of two wires. Therefore, only the measuring errors of cables and contact resistors and capacitances from the LCR meter to the switching matrix could minimize the open and short calibration.

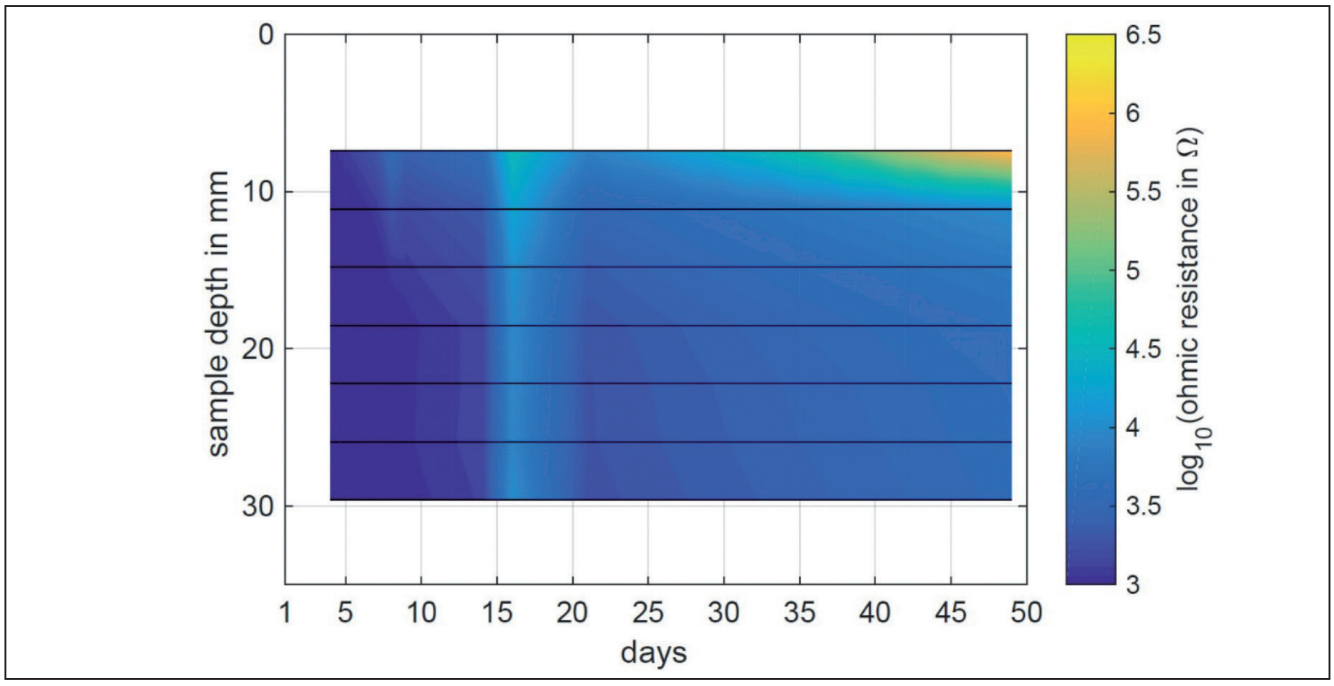

Fig. 7: Spatial and temporal distribution of the ohmic resistance for the cement based floating screed with 35 mm sample thickness presented as a two-dimensional contour plot

Fig. 7 depicts the measured ohmic resistance over time and sample depth for an alternating current frequency of 100 Hz. The seven horizontal black lines represent the geometric centre between two neighbouring metal electrodes. This position is considered as the representative measurement position. First of all, only the first 49 days are recorded. After this, the sample becomes too dry and the existing values exceed the measurement range of the used LRC-meter. As expected from the beginning,

the electrical resistance is similarly low with values of around 1000 Ω. At this stage, the pore system is over-saturated and a significant amount of liquid water is present in the pores. With progressive hydration and evaporation of the screed, the resistance increases throughout the entire sample. After day 38, the resistance between the two topmost electrodes increases exponentially. On day 49, the topmost measured resistance is almost 1 MΩ, whereas all other measurement positions show resistances below 10 kΩ. On day 16, an unexpected jump with discontinuity of all seven measured values is visible. This measurement day is probably an outlier. Nevertheless, it does not affect the data processing.

The resistance and the water layer thickness derived from the humidity measure-ments are correlated. On the one hand, the humidity sensors have to be out of saturation for a valid water layer calculation. On the other hand, resistance measurements have to exist for correlation. For the thin sample of the cement based floating screed, 29 data points exist with valid humidity measurements and corresponding measured resistances. First data points are acquired on measurement day 31. From the original 16 screed samples, only three samples show an overlap of humidity and resistance measurements at all. The other two samples have 4 and 7 valid data points. Thus, only the shown sample is described in this paper because the other samples do not have enough data points for further analyses and regression calculations.

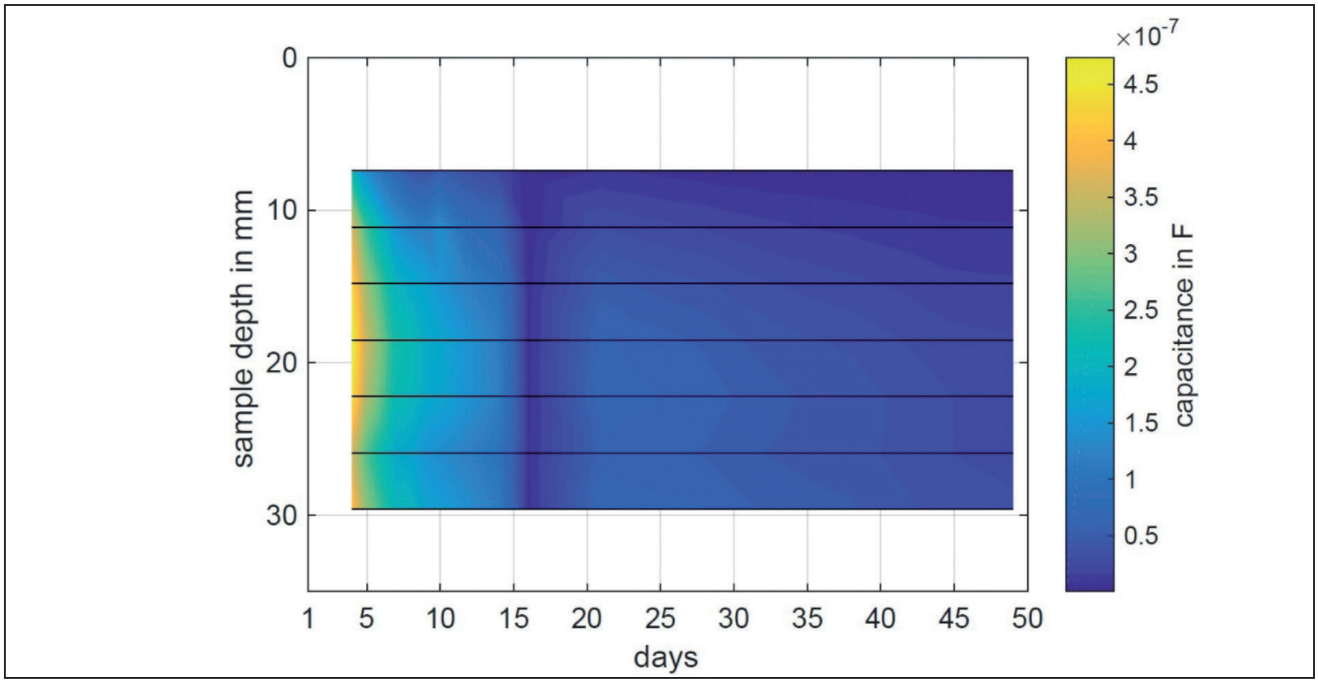

Fig 8: Spatial and temporal distribution of the capacitance for the cement based floating screed with 35 mm sample thickness presented as a two-dimensional contour plot

In **Fig. 8**, the measured capacitance is shown for an alternating current frequency of 100 Hz. Over time, the capacitance decreases. Due to hydration and evaporation, the amount of free water decreases. Thus, less water molecules are available for polarisation. All measured capacitances are below 1 µF, and on measurement day 42, the topmost electrodes already show values below 1 nF. As discussed before, the measurements on day 16 show an inconsistent behaviour.

4 Results

4.1 Water layer thickness dependence of the measured humidity

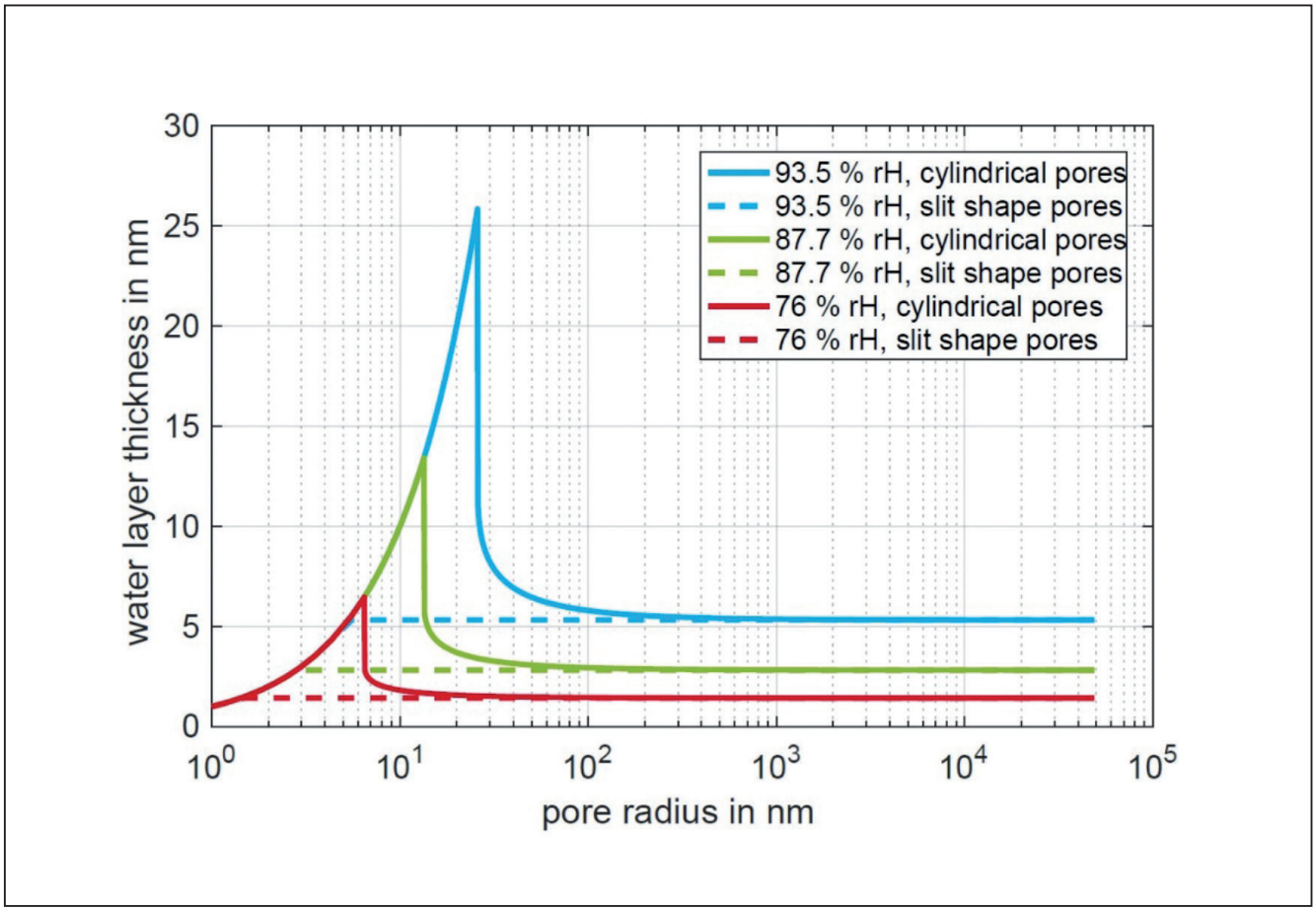

Fig 9: Calculated water layer thickness for the maximum, median, and minimum measured humidity; the slit shape and cylindrical shape pore model are illustrated for the cement based floating screed

Fig. 9 shows the predicted water layer thickness of the highest, lowest, and the median humidity. The highest water layer thickness is generated by the highest humidity of 93.5% rH. The higher the humidity, the higher

the water vapour pressure in the pores. Hence, more water molecules are adsorbed by the water layer to fulfil the thermodynamic equilibrium between the vapour and liquid phase. Thus the water layer thickness increases with humidity. For pores larger than 1 µm, the corresponding water layer thickness is approximately 5.3 nm. For the median humidity of 87.7% rH, pores larger than 1 µm have a predicted water layer thickness of 2.8 nm and for 76% rH, the thickness is 1.4 nm. For all humidity levels, two different geometric models are used. The classic BET theory assumed slit shape pores (Brunauer et al., 1938); this means, all pores are flat and no curvature exists. In this case, the predicted water layer thickness is independent of the pore size. As long as the water layer thickness is larger than the pore cross section, the pore remains fully saturated. At 93.5% rH, pores with a radius $r \leq 5.5$ nm are completely filled with water, all larger pores possess a water layer thickness of t_a = 5.3 nm. If cylindrical shaped pores are assumed as the geometric model, the water layer thickness becomes dependent on the pore radius. The water layer of a cylindrical pore is located at the fringe of the pore. Hence, the water layer has a concave curvature. This curvature influences the maximum humidity at which pore saturation is reached as well as the water vapour partial pressure at the phase transition between vapour and liquid phase. Therefore, the pores are able to incorporate more water compared to slit shape pores. For 93.5% rH, all pore with $r \leq 25.8$ nm are still fully saturated. Larger pores are moving away from full saturation, but still incorporate more water and a significant higher water layer when compared to slit shape pores. The larger the radius, the low the effect of water layer curvature. For pores larger than 1 µm, the influence of the curvature is negligible. For lower humidity, the water vapour pressure decreases, and the corresponding water layer thickness decreases as well. For 76% rH, pores larger than r = 6.4 nm are already leaving saturation. In fact, an assumed cylindrical pore model always delivers more moisture than a slit shape model. To evaluate both models, the predicted moisture is compared to the measured moisture (Strangfeld and Kruschwitz, 2018). The cylindrical pore model shows a much higher accordance to the measured moisture. Therefore, in the following, all discussed water layer data are based on a cylindrical pore model and the approach of Hillerborg.

4.2 Correlation of capacitance and moisture with the corresponding relative humidity

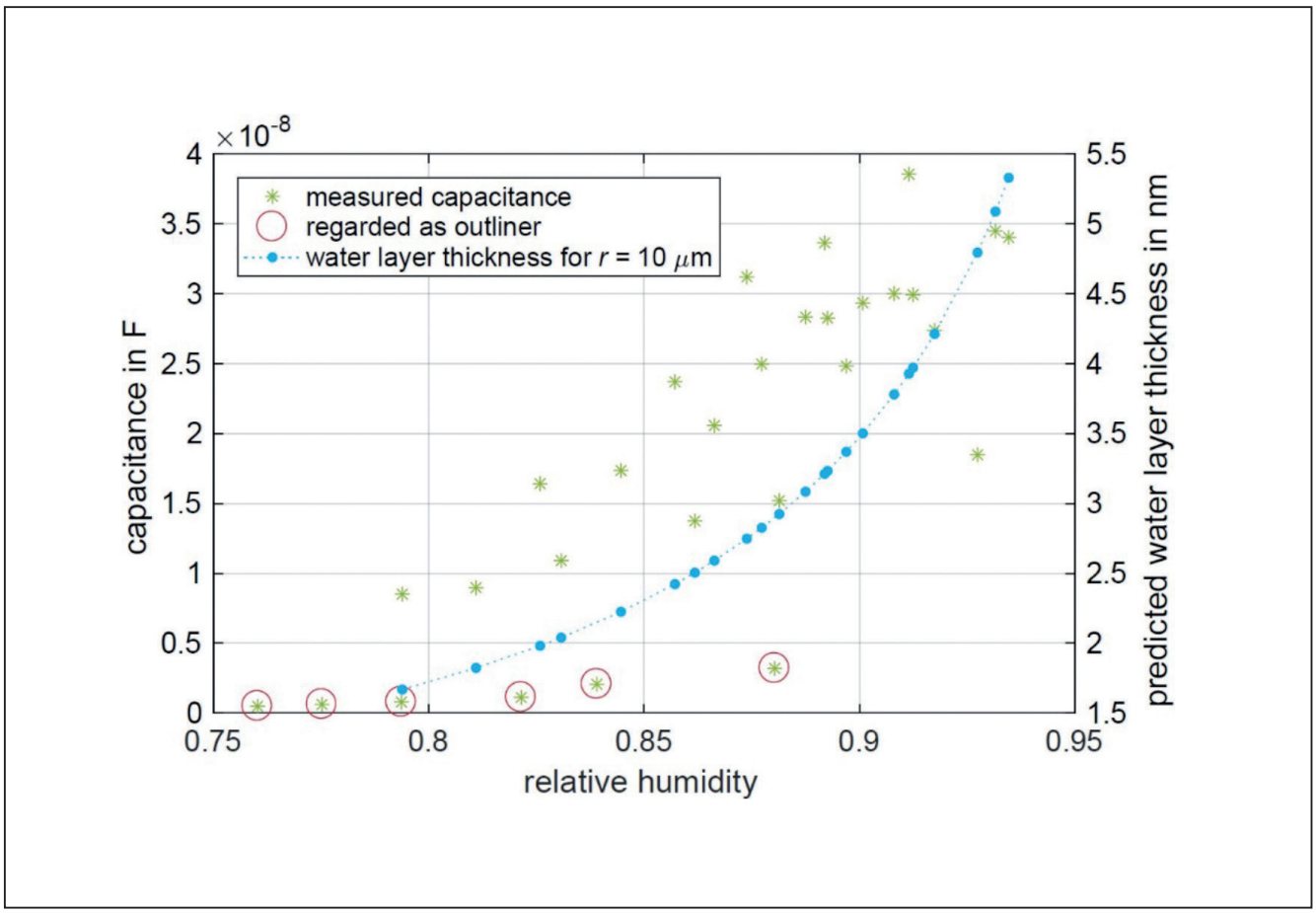

Fig 10: Correlation between the capacitance and the relative humidity measured by embedded sensors; predicted water layer thickness for cylindrical pore with r = 10 µm computed for the corresponding humidity

In **Fig. 10**, the correlation between the relative humidity and the capacitance are illustrated. Both quantities are measured based on embedded sensors. As expected, a higher humidity correlates with a higher capacitance. Nevertheless, the scatter in the data is fairly high. Furthermore, six measurement values are reduced by more than one magnitude as compared to the other data. These six points are marked by red circles. All six outliers correspond to the topmost measurement position. As discussed in the setup, for the multi-ring-electrodes, there is no distinct measurement position. The electromagnetic field incorporates a larger measurement volume around the two electrodes. Although hydration takes places everywhere in the sample, evaporation starts at the top surface. Therefore, the topmost region dries first, including high moisture gradients. It is believed that the high gradients lead to non-linear beha-

viour between measured humidity and capacitance. At a certain level of dryness, the contact resistance between electrode and screed may affect the measurement as well. Therefore, the six marked data points are considered as outliers and are excluded in the further analysis.

However, **Fig. 10** also shows the predicted water layer thickness of cylindrical pores for the corresponding humidity. As discussed in **Fig. 9**, the water layer thickness is a function of the pore radius. Thus, in **Fig. 10**, the water layer of a pore with r = 10 µm is illustrated. A smaller pore would have a higher water layer and thus, the water layer averaged over all pore radii would be higher as well. Therefore, the illustrated water layer thickness with r = 10 µm is considered as the minimum thickness. Which of the two quantities, minimum or averaged water layer, is the governing one to describe the capacitance and resistance variation has not been investigated so far. For the sake of understanding, the minimum water layer is considered in the following.

4.3 Correlation of resistance and water layer thickness

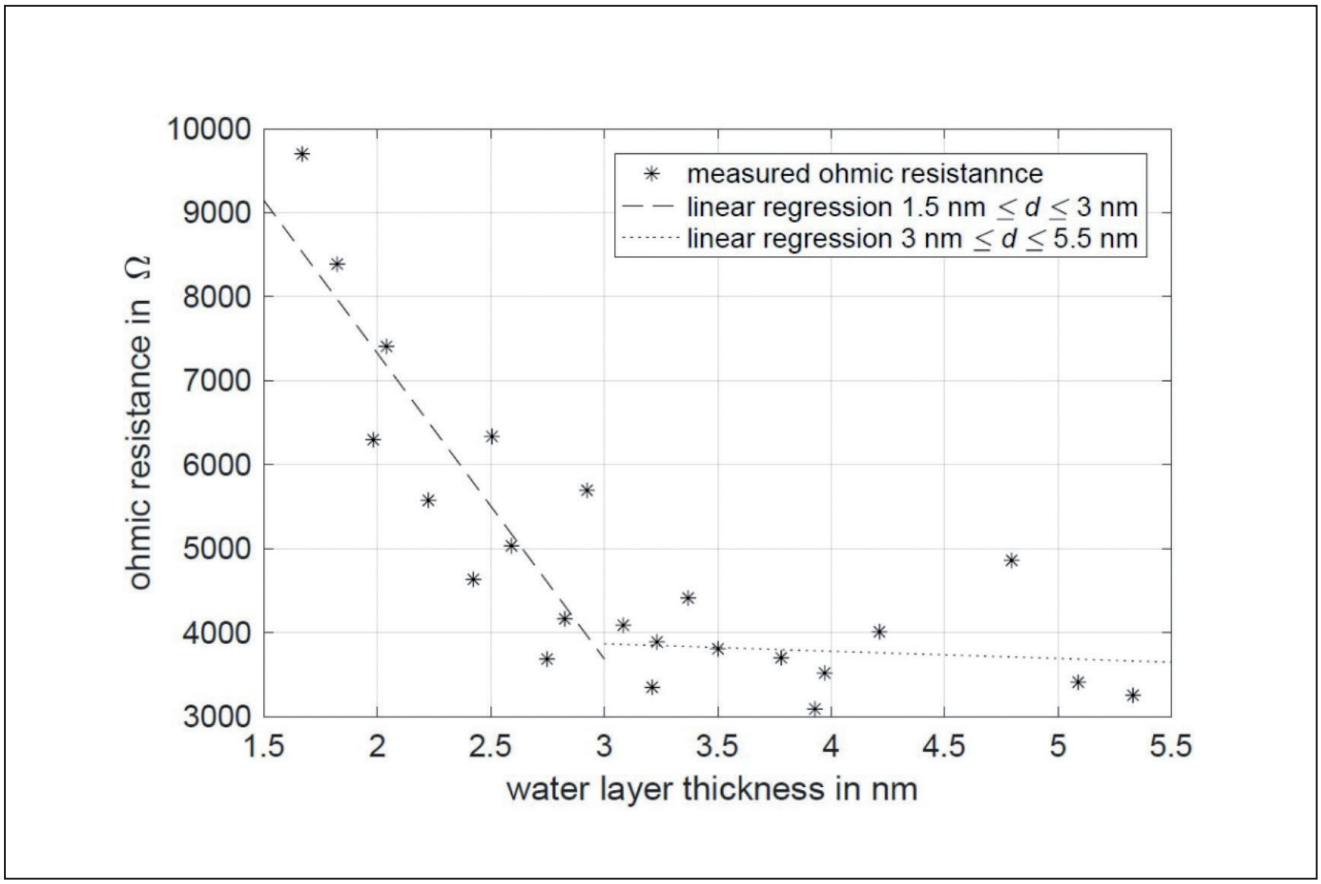

Fig 11: Correlation of the measured ohmic resistance based on embedded sensors and the calculated water layer thickness of a r = 10 µm pore for the cement based floating screed

Fig. 11 depicts the correlation between the water layer thickness d and the ohmic resistance for the remaining 23 data points. In comparison to the capacitance, the measured resistance has a lower scatter. The considered range is 1.5 nm ≤ *d* ≤ 5.5 nm which coincides with 79.4% rH and 93.5% rH, respectively. In general, lower ohmic resistance correlates with higher water layer thickness. This is expected because higher water layers include more moisture which reduces the resistance. Nevertheless, one might see a change in trend. Although 23 data points are a small dataset, at approximately *d* = 3 nm, the slope increases significantly. Hence, two linear regressions are calculated to illustrate this kink. The margin of *d* = 3 nm is selected arbitrarily by eye. The exact regression function is not discussed here due to the low number of data points, the arbitrary selection of the margin, and the possibility that a linear function does not represent the physics correctly. However, for this specific dataset, the slope decreases from ~ -3640 Ω/nm to ~ -87 Ω/nm. The change factor of the two slopes is more than one magnitude with ~ 41. A water layer of *d* = 3 nm corresponds to a relative humidity of ~ 88.3 % rH. Based on this preliminary study, the correlation between the electric resistance and the water layer thickness shows change in trend at approximately *d* = 3 nm or ~ 88.3 % rH. Further studies are required to validate this statement.

4.4 Error discussion

A detailed error discussion regarding the setup and the humidity sensors has been already presented in (Strangfeld and Kruschwitz, 2018). However, for the water layer thickness calculation, some further influences have to be discussed.

First of all, eight screed types in 16 samples were investigated. 13 of the 16 sample do not have any temporal overlap between the electric resistance measurements and the humidity measurements. Moreover, 2 of the remaining 3 samples show a weak dataset of 3 or 4 measurement points. Only the discussed cement based floating screed has a representative dataset of 29 measurement points. Nevertheless, the topmost electric resistance measurements are probably highly influenced by the strong moisture gradient. In general, a much broader dataset is required to confirm the current findings. The used dataset of 23 data points is a preliminary study which should only demonstrate the used approach. So far, the shown correlation between the water layer thickness and the electric resistance cannot be generalised.

Furthermore, the comparison between the measured sample weight and the calculated moisture content show systematic deviations between day 28 and 42 (Strangfeld and Kruschwitz, 2018). It is assumed that the hydration process exerts a significant influence during this period. This means that liquid water is not evaporated; it is chemically bound in the cement matrix. This process of hydration implicates that the pore system is still changing as well as the pore volume distribution. A separation of hydration and evaporation is not possible with the current data set. In a future study, the samples may hydrate fully saturated for at least two months. This should reduce the influence of hydration during the humidity measurements and the prediction of the sample moisture.

Regarding the water layer thickness calculation, two major aspects have to be taken into account. In **Fig. 11**, only the water layer thickness of a r = 10 µm pore is used. Nevertheless, smaller pores have a higher water layer, as shown in **Fig. 9**. Thus, the real water layer thickness varies depending on the pore radius. Small pores are completely saturated and show a much higher water layer. Which water layer thickness is representative for a partially saturated heterogeneous pore system is still an open question. More measurement points are required for a detailed evaluation.

A further systematic deviation of the water layer thickness calculation is the hysteresis of the sorption isotherm. The shown measurement data are recorded during the desorption of the cement based floating screed. During desorption, inkbottle water has a major influence on the materials moisture. Inkbottle water describes water which is trapped in larger pores. These larger pores would only be partially saturated during adsorption. If these larger pores are connected to the pore system via only smaller pores, these larger pores remain fully saturated until the smaller connection pores leave saturation as well. For the considered cement based floating screed, the amount of inkbottle water is approximately twice the amount of capillary water (Strangfeld and Kruschwitz, 2018). To derive a representative water layer thickness is even more complicated for desorption. In a future study, desorption as well as adsorption have to be monitored. Especially during adsorption, only capillary water exists and all larger pores are partially saturated without any inkbottle water.

5 Conclusion and Outlook

The discussed sample is a cement based floating screed with a height of 35 mm. Five humidity sensors and eight electrodes are embedded in the screed to monitor the spatial humidity distribution. Furthermore, the sample weight and the pore volume distribution are measured. With the approach of Hillerborg, the moisture of the sample is predicted based on a pore model with cylindrical pores during evaporation. Furthermore, this approach yields the pore saturation as well. Therefore, the water layer thickness of the partially saturated pores is calculated. By means of the multi-ring-electrode, the electric impedance is measured. The real and complex part of the impedance are evaluated and correlated with the relative humidity measurements and the corresponding water layer thickness. Water layers with a thickness of 1.5 nm up to 5.5 nm were derived from the humidity measurements. Based on the small data set of 23 measurement points, a significant change in trend is visible. The slope between the real part of the impedance in the water layer thickness range of 1.5 nm to 3 nm is approximately 40 times higher as the slope in the range of a water layer thickness between 3 nm to 5.5 nm. The 3 nm threshold corresponds to a corresponding relative humidity of around 88.3% rH.

To improve the measurements in a future study, screed samples have to be investigated during desorption as well as adsorption. For further investigation of correlation between the complex resistance and the water layer thickness the measurement setup must be improved. It is planned to use a 2-pole switching matrix and completely connect all signal paths from the LCR meter to the MRE with four wire to minimize measuring errors. Furthermore, the influence of hydration should be reduced to a minimum.

Based on these improved measurements, one might be able to determine a clear correlation between the water layer thickness and the electric impedance. This may disclose the effect of polarisation of water molecules in thin water layers. Interaction of the first monomolecular water layer with the cement matrix and hydrogen bridge bonds in the further water layer are supposed to cause the non-linear increase of electric impedance at low moisture levels. In the future, our approach might be able to quantify this effect.

References

Barrett, E. P., Joyner, L. G. and Halenda, P. P. (1951) The determination of pore volume and area distributions in porous substances. Computations from nitrogen isotherms. Journal of the American Chemical Society, 73, 373–380.

Brunauer, S., Emmett, P. H. and Teller, E. (1938) Adsorption of gases in multimo-lecular layers. Journal of the American Chemical Society, 60, 309–319.

Chaube, R. P. (1994) A study of the moisture transport process in concrete as a composite material. Proceedings of the Japan Concrete Institute, 16, 895–900.

DIN 66134 (1998) Bestimmung der Porengrößenverteilung und der spezifischen Oberfläche mesoporöser Feststoffe durch Stickstoffsorption, Deutsche Norm.

ISO 15901-2 (2006) Pore size distribution and porosity of solid materials by mercury porosimetry and gas adsorption - Part 2: Analysis of mesopores and macropores by gas adsorption, International Standard.

Halsey, F. (1948) Physical adsorption on non-uniform surfaces. The Journal of Chemical Physics, 16, 931–937.

Hase, F. (2016) Design und Aufbau verschiedener Messsysteme zur Ermittlung des Feuchtigkeitsprofiles von Estrich. Master Thesis, HTW Berlin.

Hillerborg, A. (1985) A modified absorption theory. Cement and Concrete Research, 15, 809–816.

Kruschwitz, S. (1985) Assessment of the complex resistivity behavior of salt affected building materials. PhD thesis, Technische Universität Berlin.

Morris, W., Vico, A., Vazquez, M., de Sanchez, S.R (2002) Corrosion of reinforcing steel evaluated by means of concrete resistivity measurements, Corrosion Science, 44, 81–99.

Nürnberger, U. (1995) Korrosion und Korrosionsschutz im Bauwesen. Band 1 und 2. Bauverlag Wiesbaden/Berlin.

Sodeikat, C. (2010), Feuchtesensoren in der Bauwerksüberwachung. Beton- und Stahlbetonbau, 105, 770–777.

Strangfeld, C. and Kruschwitz, S. (2018) Monitoring of the absolute water content in porous materials based on embedded humidity sensors. Construction and Building Materials, 177, 511–521.

Strangfeld, C., Kruschwitz, S., Wöstmann, J., Nagel, S., Hase, F. (2016) Moisture in screed: a non-destructive multi-sensor approach. 8th European Workshop on Structural Health Monitoring, 1–11.

Strangfeld, C., Prinz, C., Hase, F., Kruschwitz, S. (2018) Data of embedded humidity sensors, sample weights, and measured pore volume distribution for eight screed types. Data in Brief, 21, 8–12.

Thomson, W (1871) LX. On the equilibrium of vapour at a curved surface of liquid. The London, Edinburgh, and Dublin Philosophical Magazine and Journal of Science, 42, 448–452.

Washburn, E. W. (1921) The dynamics of capillary flow. Physical Review, 17, 273–283.

Weise, F., Voland, K., Pirskawetz, S. and Meinel, D. (2012) Analyse AKR-induzierter Schädigungsprozesse in Beton. Beton- und Stahlbetonbau, 107, 805–815.